Present-day irrigation mitigates heat extremes

Wim Thiery[1,2] (ID), **Edouard L. Davin**[1], **David M. Lawrence**[3] (ID), **Annette L. Hirsch**[1] (ID), **Mathias Hauser**[1] (ID), and **Sonia I. Seneviratne**[1] (ID)

[1]Institute for Atmospheric and Climate Science, ETH Zurich, Zurich, Switzerland, [2]Department of Hydrology and Hydraulic Engineering, Vrije Universiteit Brussel, Brussels, Belgium, [3]National Center for Atmospheric Research, Boulder, Colorado, USA

Correspondence to:
W. Thiery,
wim.thiery@env.ethz.ch

Abstract Irrigation is an essential practice for sustaining global food production and many regional economies. Emerging scientific evidence indicates that irrigation substantially affects mean climate conditions in different regions of the world. Yet how this practice influences climate extremes is currently unknown. Here we use ensemble simulations with the Community Earth System Model to assess the impacts of irrigation on climate extremes. An evaluation of the model performance reveals that irrigation has a small yet overall beneficial effect on the representation of present-day near-surface climate. While the influence of irrigation on annual mean temperatures is limited, we find a large impact on temperature extremes, with a particularly strong cooling during the hottest day of the year (-0.78 K averaged over irrigated land). The strong influence on extremes stems from the timing of irrigation and its influence on land-atmosphere coupling strength. Together these effects result in asymmetric temperature responses, with a more pronounced cooling during hot and/or dry periods. The influence of irrigation is even more pronounced when considering subgrid-scale model output, suggesting that local effects of land management are far more important than previously thought. Our results underline that irrigation has substantially reduced our exposure to hot temperature extremes in the past and highlight the need to account for irrigation in future climate projections.

1. Introduction

Over 70% of the world's land surface is presently under direct human management [*Luyssaert et al.*, 2014]. Using land resources in fulfillment of their needs, humans have either altered land surface properties (land cover changes) or modified characteristics of the existing land cover (land management changes), in some cases with harmful effects [e.g., *Jacobs et al.*, 2016a, 2016b]. Irrigation counts among the most widely applied land management technique and is an essential contributor to global food production. Although representing only ~2% of the global land surface [*Siebert et al.*, 2005], irrigated land accounts for over 40% of the global food production [*Lobell et al.*, 2006b; *Bonfils and Lobell*, 2007]. Throughout the last century, irrigation amounts have grown rapidly, with estimated total volumes increasing from around 500 km^3 yr^{-1} at the start of the twentieth century to between 2200 and 3000 km^3 yr^{-1} around the year 2000 [*Shiklomanov*, 2000; *Döll and Siebert*, 2002; *Siebert and Döll*, 2007; *Hanasaki et al.*, 2008; *Wisser et al.*, 2010]. In the future, land management is expected to expand and intensify to meet growing demand for food, fiber, and energy [*Foley et al.*, 2011]. However, projected climate change caused by both anthropogenic greenhouse gas emissions and land use activities is likely to constrain an increase in irrigation.

Human land use activities have resulted in large changes to the biogeochemical and biogeophysical properties of the Earth surface, with profound implications for the climate system. Besides land cover changes, whose climatic consequences have been much studied in recent decades [e.g., *Pongratz et al.*, 2009a, 2009b; *Akkermans et al.*, 2014], land management changes have recently been advanced as another important human influence on the climate system. Analysis of ground measurements and remote sensing observations has shown that the aggregated impact of land management on surface temperature is of similar magnitude to that of land use change [*Luyssaert et al.*, 2014]. Some land management practices were also identified as having the potential to either mitigate or aggravate climate extremes. For instance, *Davin et al.* [2014] showed how the enhanced surface albedo following suppressed tillage has a beneficial effect on European heat wave intensity. Likewise, *Doughty et al.* [2011] and *Wilhelm et al.* [2015] advocate that the use of brighter crops may reduce summertime maximum daily temperatures at high latitudes. To assess the biogeophysical effects of

land cover and land management changes in a multimodel framework, the Land Use Model Intercomparison Project [*Lawrence et al.*, 2016] was launched very recently within the framework of the Coupled Model Intercomparison Project phase 6 (CMIP6).

Irrigation is the land management practice with perhaps the largest effect on climate [*Sacks et al.*, 2009]. The biogeophysical impacts of irrigation have been investigated in several regional climate modeling studies [e.g., *Haddeland et al.*, 2006; *Kueppers et al.*, 2007; *Kueppers and Snyder*, 2012; *Saeed et al.*, 2009, 2013; *Lu and Kueppers*, 2015a; *Lu et al.*, 2015b]. While using different irrigation implementations for different regions of the world, all of the regional studies report a cooling of the near-surface air in response to irrigation. Estimates of irrigation induced cooling in global climate model (GCM) studies remain uncertain, with reported impacts averaged over all land ranging from −0.15 K to +0.02 K [*Boucher et al.*, 2004; *Sacks et al.*, 2009; *Puma and Cook*, 2010; *Cook et al.*, 2015].

A number of challenges arise when representing irrigation in a GCM. (i) First, the applied amount of irrigation water needs to be realistic. This may be achieved either by prescribing historically observed irrigation amounts or by meeting crop water demands based on physical principles. Whereas the former strategy might be preferred when observed irrigation rates are available at high spatiotemporal resolution, the latter is useful in the absence of such data or when simulating future changes. (ii) Second, land surface models (LSMs) in GCMs should be capable of realistically simulating crop responses to irrigation. This requires explicit crop representation in LSMs, preferably on a separate soil column. Irrigated water can then be applied to the irrigated crop fraction of the grid cell only. (iii) Third, separating irrigation impacts from other effects, notably natural variability, is essential to investigate the two-way interactions between climate and irrigation. Internal variability may explain part of the impacts reported in previous modeling studies based on a single member, notably influences in regions at great distance from the applied forcing [e.g., *Boucher et al.*, 2004; *Sacks et al.*, 2009; *Puma and Cook*, 2010; *Cook et al.*, 2011] and counter-intuitive effects such as a global mean warming [e.g., *Sacks et al.*, 2009] or substantial warming in India [e.g., *Boucher et al.*, 2004]. This may also explain why dynamical and remote responses to irrigation are often inconsistent across GCM simulations [*Cook et al.*, 2011]. (iv) Finally, it needs to be determined whether representing irrigation improves the skill of the GCM in the present-day climate. This is particularly challenging for climate extremes, as the limited number of global observational data sets complicate a comprehensive model evaluation.

The main goal of this study is therefore to assess the climatic impacts of irrigation with particular attention to climate extremes and the physical mechanisms underlying these impacts. This is achieved by addressing the aforementioned challenges in the following way: (i) We apply a recent irrigation parameterization whereby actual irrigation quantities are computed based on local crop water demands but constrained by global observed irrigation amounts [*Oleson et al.*, 2010]. This approach holds a good balance between applying actual irrigation observations [*Boucher et al.*, 2004; *Sacks et al.*, 2009; *Puma and Cook*, 2010; *Cook et al.*, 2011, 2015] and completely removing crop water stress [*Lobell et al.*, 2006a; *Kueppers et al.*, 2007; *Kueppers and Snyder*, 2012; *Döll and Siebert*, 2002; *Saeed et al.*, 2009], the latter implying an overestimation of actual irrigation amounts. (ii) This parameterization was implemented in version 4.0 of the Community Land Model (CLM4) [*Oleson et al.*, 2010]. In CLM4, irrigation is applied to the irrigation crop fraction placed on a separate soil column, and the applied water is extracted from runoff, thereby closing the hydrological balance. (iii) We conduct ensemble simulations to limit the effects of natural variability on our results. (iv) Finally, we pay special attention to model evaluation, in particular by using global remote sensing and in situ observational data sets to assess the model's ability to reproduce observed irrigation quantities, the near-surface climate and precipitation. Adopting one or more of the above challenges may improve the representation of surface freshwater within a climate model, as demonstrated in several recent studies [e.g., *Lobell et al.*, 2009; *Cook et al.*, 2015; *Thiery et al.*, 2014a, 2014b, 2015, 2016]. In addition to aforementioned improvements, our study is the first (i) to investigate the impacts of irrigation on climate extremes from a global perspective, (ii) using global climate experiments at an unprecedented spatial resolution of about 1°, (iii) to systematically decompose the irrigation impact on the surface energy balance, and finally, (iv) to consider irrigation influences at the subgrid scale.

In this paper, we first assess the added value of incorporating irrigation in present-day GCM simulations. The impacts of irrigation on climatic means and extremes are subsequently quantified by comparing ensemble simulations including irrigation to ensemble simulations where irrigation is switched off. This influence is then

investigated in more detail by applying a surface energy balance decomposition technique and studying the local versus regional effects induced by irrigation.

2. Model and Methods

2.1. CESM and Irrigation Implementation

To investigate the influence of irrigation on climate extremes, we use version 1.2 of the Community Earth System Model (CESM1.2, hereafter referred to as CESM), a fully coupled, state-of-the-art GCM [*Hurrell et al.*, 2013]. This model applies version 5.3 of the Community Atmosphere Model (CAM5) to compute atmospheric processes, whereas the land surface is represented by version 4.0 of the Community Land Model (CLM4) [*Oleson et al.*, 2010; *Lawrence et al.*, 2011]. CLM4 includes an explicit treatment of photosynthesis which controls stomatal conductance. Furthermore, individual land pixels can be composed of multiple land units due to the nested tile approach, which enables the implementation of multiple soil columns and represents biomes as a combination of different plant functional types.

The interactive irrigation module in CLM4 is described in detail by *Oleson et al.* [2013] and summarized hereafter. Irrigation in CLM4 is implemented for C3 generic crops only, and irrigation rates depend on the vegetation state and the simulated soil moisture content (w, kg m^{-2}). When the irrigation option is enabled, irrigated and rainfed crop fractions of each pixel are subdivided according to a high-resolution global data set (Figure 1) [*Siebert et al.*, 2005]. Irrigation areas are thus correctly represented by design. Irrigated crops are subsequently placed on a separate soil column to avoid irrigation water affecting other plant functional types (PFTs). Irrigation is activated only if water is limiting photosynthesis during the growing season [*Leng et al.*, 2013].

For each soil layer in the irrigated crop tile, the deficit between the actual and a target soil moisture content is replenished on a daily basis. The target soil moisture content in each soil layer i ($w_{\text{target},i}$, kg m^{-2}) is computed at 6 A.M. local time from the crop's water demands and soil saturation in such a way that the global annual water amount added through irrigation matches present-day observed gross irrigation water use. In particular, $w_{\text{target},i}$ is the weighted average of (i) the minimum w eliminating water stress in that layer ($w_{o,i}$, kg m^{-2}) and (ii) the saturated w in that layer ($w_{\text{sat},i}$, kg m^{-2}):

$$w_{\text{target},i} = (1 - 0.7) * w_{o,i} + 0.7 * w_{\text{sat},i} \tag{1}$$

The value 0.7 was chosen empirically to match global, annual irrigation amounts in CLM4 with values observed around the year 2000 (section 1). The total water deficit (w_{deficit}, kg m^{-2}) of the soil column is then obtained as the sum of all potential water deficits over the soil layers containing roots (topmost unfrozen layers only). An amount equal to w_{deficit} is subsequently removed from total liquid runoff and applied directly to the ground surface. This approach mimics extraction from nearby rivers but without imposing a limitation on water availability (i.e., runoff can have a negative value).

2.2. Experimental Design

We run CESM to generate two climate ensembles. First, a five-member control ensemble (hereafter referred to as CTL) is conducted without irrigation. The second five-member ensemble (hereafter referred to as IRR) is identical to the control experiment, except that the irrigation module is switched on. Model results are analyzed over global land and global irrigated land areas (excluding Antarctica) and highlighted for those regions where substantial irrigation activities are recorded: western North America (WNA), central North America (CNA), south Europe and Mediterranean (MED), West Asia (WAS), South Asia (SAS), Southeast Asia (SEA), and East Asia (EAS; Figure 1a). The regions were originally defined in the Intergovernmental Panel on Climate Change (IPCC) Special Report on Managing the Risks of Extreme Events and Disasters to Advance Climate Change Adaptation (SREX) [*Seneviratne et al.*, 2012]. We assume pixels to be irrigated if the irrigated fraction exceeds 10% of the total grid cell area, thus excluding pixels for which only limited influence is expected.

All simulations cover the period 1976–2010 (35 years), of which the first 5 years are considered as spin-up time and excluded from the analysis. On 1 January 1976, we imposed small random perturbations on the order of 10^{-14} K to the initial temperature field. This way each ensemble contains five unique realizations in terms of natural variability but with an identical representation of the underlying physical processes [*Perkins and Fischer*, 2013]. We conducted our simulations at a horizontal resolution of 0.90° × 1.25°, with prescribed transient monthly sea surface temperatures and sea ice fractions from the data set described by *Hurrell et al.* [2008].
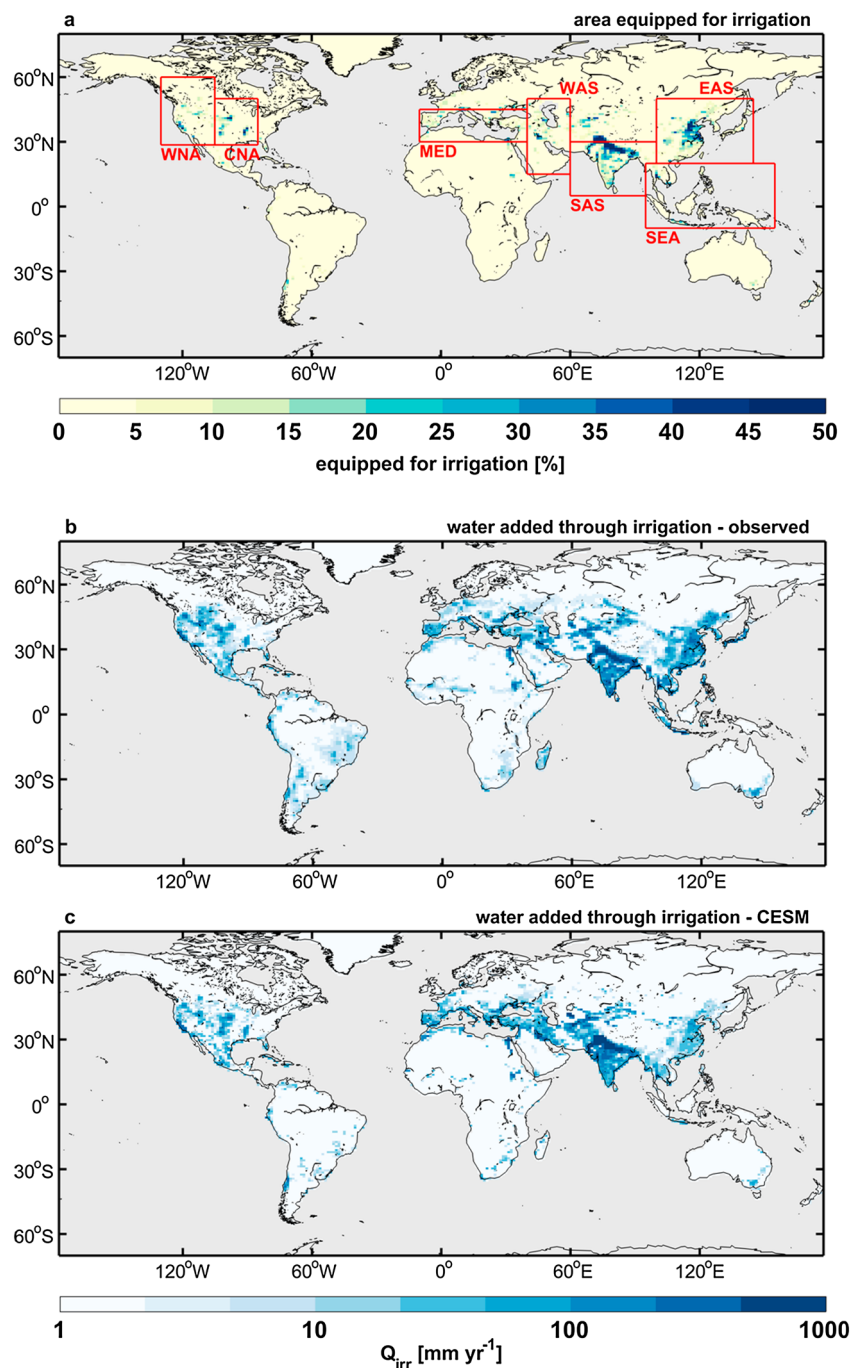
Figure 1. (a) Percentage of each grid cell equipped for irrigation (%) [*Siebert et al.*, 2005]. Annual irrigation rates Q_{irr} (mm yr^{-1}; log scale) as (b) observed around 2000 [*Helkowski*, 2004; *Sacks et al.*, 2009] and (c) simulated by CESM from 1981–2010.

Sea surface temperatures were prescribed to focus on land-atmospheric interactions without the added complexity of ocean-atmosphere feedbacks in the climate system. In addition, transient greenhouse gas concentrations were prescribed from measurements, and satellite-based observations of vegetation phenology were imposed in CLM4. As such our CTL ensemble closely resembles the setup adopted for the CESM1.0 simulations conducted within the framework of the Atmospheric Model Intercomparison Project (AMIP). One exception is, however, land use, where we assumed static land cover corresponding to the year 2000 to be technically able to switch on the irrigation module.

Table 1. Data Products Used for Model Evaluation (SRes: Spatial Resolution; TRes: Temporal Resolution; Q_{irr}: Irrigation Rates; LHF: Latent Heat Flux; SHF: Sensible Heat Flux; SW_{net}: Surface Net Shortwave Radiation; LW_{net}: Surface Net Longwave Radiation; T_{mean}: Near-Surface Temperature; P: Precipitation; TXx: Annual Maximum Daytime Temperature; and TNn: Annual Minimum Nighttime Temperature)

Variable (Units)	Data Set	Version	Source	SRes	TRes	Years	References
Q_{irr} (mm yr^{-1})	AQUASTAT	1	census	0.5° × 0.5°	annual	2000	*Helkowski* [2004]
LHF (W m^{-2})	LandFlux-EVAL	1	mixed	1.0° × 1.0°	monthly	1989–2005	*Mueller et al.* [2013]
	GLEAM	3.0a	mixed	0.25° × 0.25°	daily	1981–2010	*Miralles et al.* [2011]
	Fluxnet-MTE	1	stations	0.5° × 0.5°	monthly	1982–2010	*Jung et al.* [2010]
SHF (W m^{-2})	FLUXNET-MTE	1	stations	0.5° × 0.5°	monthly	1982-2010	*Jung et al.* [2010]
SW_{net} (W m^{-2})	GEWEX-SRB	REL3.0	satellite	1.0° × 1.0°	monthly	1984–2007	*Stackhouse et al.* [2011]
LW_{net} (W m^{-2})	GEWEX-SRB	REL3.1	satellite	1.0° × 1.0°	monthly	1984–2007	*Stackhouse et al.* [2011]
T_{2m} (K)	CRU	3.22	stations	0.5° × 0.5°	monthly	1981–2010	*Harris et al.* [2014]
P (mm/month)	CRU	3.22	stations	0.5° × 0.5°	monthly	1981–2010	*Harris et al.* [2014]
	GPCP	2.2	mixed	2.5° × 2.5°	monthly	1981–2010	*Huffman et al.* [2001]
TXx (K)	GHCNDEX	1	stations	2.5° × 2.5°	monthly	1981–2010	*Donat et al.* [2013a]
TXx (K)	HadEX	2	stations	2.5° × 3.75°	monthly	1981–2010	*Donat et al.* [2013b]
TNn (K)	GHCNDEX	1	stations	2.5° × 2.5°	monthly	1981–2010	*Donat et al.* [2013a]
TNn (K)	HadEX	2	stations	2.5° × 3.75°	monthly	1981–2010	*Donat et al.* [2013b]

2.3. Evaluation Data Sets

The performance of the CTL and IRR ensembles is assessed by comparing model output to observational products for various quantities (see Table 1 for their technical specifications). To start, we pay particular attention to CLM4's ability to reproduce observed irrigation amounts by comparing it to census data compiled by the Food and Agricultural organization of the United Nations (FAO) and disaggregated on a grid (AQUA-STAT) [*Helkowski*, 2004; *Sacks et al.*, 2009]. For temperature and precipitation, we use gridded data sets from the Climate Research Unit (CRU) [*Harris et al.*, 2014] and the Global Precipitation Climatology Project (GPCP) [*Huffman et al.*, 2001]. The surface net shortwave (SW_{net}) and longwave (LW_{net}) radiation were compared to satellite-derived values available from the Global Energy and Water Cycle Exchanges Project Surface Radiation Budget (GEWEX-SRB) [*Stackhouse et al.*, 2011], while latent heat flux (LHF) and sensible heat flux (SHF) were evaluated using observations from the Fluxnet Model Tree Ensembles data set (Fluxnet-MTE) [*Jung et al.*, 2010]. In addition, LHF was also checked against the benchmark synthesis of available diagnostic evapotranspiration estimates (LandFlux-EVAL) [*Mueller et al.*, 2013] and the Global Land Evaporation Amsterdam Model (GLEAM) [*Miralles et al.*, 2011]. Finally, the annual maximum daytime temperature (TXx) and the annual minimum nighttime temperature (TNn) were compared to the daily Global Historical Climatology Network extremes data set (GHCNDEX) [*Donat et al.*, 2013a] and to the Hadley Centre extremes data set (HadEX2) [*Donat et al.*, 2013b].

We conduct our model evaluation over the period when the gridded data sets are available: 1989–2005 for LandFlux-EVAL data set, 1982–2010 for the Fluxnet-MTE product, and 1984–2007 for the GEWEX-SRB data set, whereas evaluation using AQUASTAT, CRU, GPCP, GHCNDEX, and HadEX2 covers the entire analysis period. No height correction, gap filling, or other modifications were applied to the data sets. All observational products were remapped to the CESM grid using second-order conservative remapping [*Jones*, 1999].

2.4. Extreme Indices

To assess the influence of irrigation on climate extremes, we compute a number of indices representing climate extremes from our model output. These indices are (i) the annual maximum daytime temperature TXx; (ii) the annual minimum nighttime temperature TNn; (iii) the largest number of consecutive dry days CDD, with dry days defined as days with 24 h accumulated precipitation below 1 mm; and (iv) the Heat Wave Duration Index, HWDI, that is, the number of days where, in intervals of at least six consecutive days, daily maximum temperatures exceed the 1981–2010 average, daily maximum temperature by 5 K.

2.5. Surface Energy Balance Decomposition

The energy balance at the surface-atmosphere interface can be written as

$$\epsilon \sigma T_s^4 = (1 - \alpha)SW_{in} + LW_{in} - LHF - SHF - R \qquad (2)$$

where ϵ is the surface emissivity; σ the Stefan-Boltzmann constant (5.67×10^{-8} W m^{-2} K^{-4}); T_s the surface temperature; α the surface albedo with respect to shortwave radiation; SW$_{in}$ the incoming shortwave radiation; LW$_{in}$ the incoming longwave radiation; LHF and SHF the turbulent fluxes of latent heat and sensible heat, respectively; and R the residual term, combining subsurface storage and conductive heat fluxes as well as anthropogenic heat sources arising from air conditioning and space heating.

We investigate the processes underlying the surface temperature response to irrigation using a surface energy balance decomposition method developed by *Juang et al.* [2007] and further modified by *Luyssaert et al.* [2014]. The method consists of decomposing the net impact on surface temperature arising from a given land cover or land management change into direct contributions of modified biogeophysical processes (such as surface reflection and evapotranspiration) and indirect contributions due to atmospheric feedbacks (such as cloud-radiative feedbacks). Several recent studies have successfully applied this method to CLM output [e.g., *Akkermans et al.*, 2014; *Thiery et al.*, 2015; *Vanden Broucke et al.*, 2015].

The change in surface temperature ΔT_s is decomposed by calculating the total derivative of equation (2) and solving for ΔT_s (assuming constant $\epsilon = 1$):

$$\Delta T_s = \frac{1}{4\sigma T_s^3} \left(-\text{SW}_{in}\Delta\alpha + (1-\alpha)\Delta\text{SW}_{in} + \Delta\text{LW}_{in} - \Delta\text{LHF} - \Delta\text{SHF} - \Delta R \right) \tag{3}$$

Note that here T_s denotes the surface radiative temperature at which the biogeohydrosphere complex emits longwave radiation to the atmosphere. All terms in equation (3) can be computed from the difference between both ensemble means (IRR minus CTL).

3. Results

3.1. Model Evaluation

Observed irrigation rates are reasonably reproduced by the IRR ensemble in terms of spatial patterns (Figures 1b–1c). In particular, the model captures the higher irrigation quantities in the Indo-Gangetic Plain, associated with the extensive irrigation areas in this region (Figure 1a). When spatially averaged, annual irrigation amounts are well reproduced over most SREX regions, especially over South Asia (Figure 2). This suggests that CLM4 is generally able to represent irrigation over cropland areas. In contrast, irrigation rates are strongly underestimated over East and Southeast Asia. This underestimation is possibly because CLM4 considers only one single irrigated crop type and thus applies a generic soil moisture deficit computation (section 2.1) to the irrigation-intensive rice cultures of those regions. Although South Asia also has prominent rice cultivation, these cultures require relatively less irrigation compared to, e.g., wheat crops [*Biemans et al.*, 2016], since rice fields are typically located in the wettest part of the subcontinent. Moreover, a set of offline sensitivity experiments which set the weighting factor in equation (1) to values of 0.0, 0.3, 0.7, and 1.0, respectively [see also *Leng et al.*, 2015], indicates relatively little change in modeled absolute irrigation quantities in EAS and SEA, in contrast to other regions where modeled absolute irrigation amounts are greatly affected. This suggests that the underestimation in EAS and SEA is not related to a structural deficiency in the target soil moisture computation but rather to the general representation of the land cover characteristics or background climate. We finally note that model and reference are not entirely independent, as annual global gross irrigation amounts derived from the AQUASTAT database (2664 km^3 yr^{-1} [*Helkowski*, 2004; *Sacks et al.*, 2009]) were used to derive the empirical coefficient in equation (1). Indeed, the global irrigation amount computed by the IRR ensemble (2288 $\pm$ 103 km^3 yr^{-1}) falls within the range marked by observational uncertainty (section 1). Nevertheless, since spatiotemporal irrigation patterns (Figures 1 and 2) were computed independently from the AQUASTAT data set, these model features can be evaluated.

Model biases and spatiotemporal root-mean-square error (RMSE) values relative to global observational products are listed in Table 2. The simulations substantially overestimate mean land precipitation by $\sim$37–102 mm yr^{-1}, although the biases demonstrate strong spatial heterogeneity. On average CESM also overestimates the evaporative fraction; that is, it overestimates LHF by $\sim$1–4 W m^{-2} while underestimating SHF by $\sim$5 W m^{-2}. These model errors are particularly large in the tropics and Australia (not shown). The CTL ensemble furthermore demonstrates an average cold bias of -0.41 K over land. This bias is dominated by large errors over the Greenland ice sheet (not shown), which might be related to issues in the model's representation of polar clouds over this region [*Van Tricht et al.*, 2016]. While having a slight cold bias on average over global land, CESM is consistently too warm over irrigated areas, both under mean and extreme conditions.
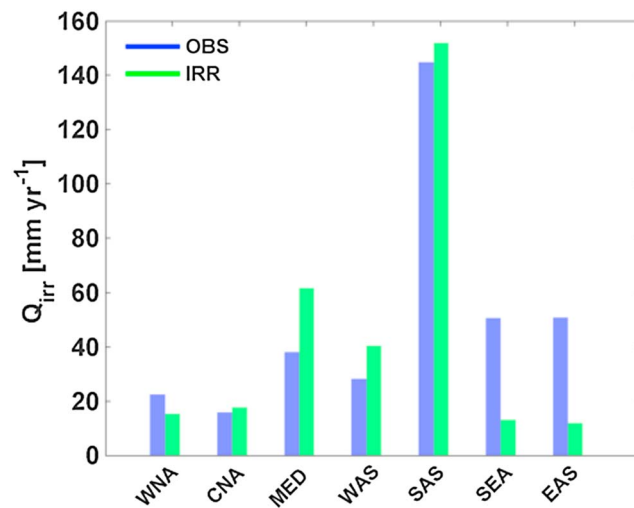
Figure 2. Annual irrigation rates Q_{irr} (mm yr^{-1}) averaged over the SREX regions as observed around 2000 [*Helkowski*, 2004; *Sacks et al.*, 2009] and simulated by CESM from 1981–2010.

Interestingly, switching on the irrigation module substantially reduces the warm bias found over irrigated areas in the CTL ensemble (Table 2). In contrast, the positive LHF bias is enhanced in the IRR ensemble as irrigation leads to an increase in evaporation. We check the added value of including irrigation in a systematic way by computing the percentage change in spatiotemporal RMSE for 12 observational products and over the SREX regions containing substantial irrigation as well as over global land and global irrigated land (Figure 3). In general, spatiotemporal RMSE values decrease for 77 out of a total of 100 considered samples (77%), with an average RMSE decrease of 3%. Over irrigated land, an improvement is found for all considered observational products except GLEAM, whereas over global land the model skill improves for all variables except TNn (Figure 3; Table 2). Thus, while the enhanced skill is small in absolute terms, it is consistent across a wide range of climatic variables and relevant spatial domains. A notable exception is the degraded representation of LHF

Table 2. Bias and Spatiotemporal RMSE of the CTL and IRR Ensemble Mean (Section 2.2) Versus Various Observational Products (See Table 1 for An Overview)[a]

Physical Quantity (Units)	All Land Bias		Irrigated Land Bias		All Land RMSE		Irrigated Land RMSE	
	CTL	IRR	CTL	IRR	CTL	IRR	CTL	IRR
Census Q_{irr} (mm yr^{-1})	−15.5	−1.8	−200.4	12.6	62.0[b]	47.7[b]	268.9[b]	247.7[b]
LandFlux-EVAL LHF (W m^{-2})	0.9	1.1	1.7	5.5	14.8	14.6	14.6	14.3
GLEAM LHF (W m^{-2})	1.9	2.1	5.6	9.3	16.2	16.2	16.9	18.8
FLUXNET-MTE LHF (W m^{-2})	4.1	4.4	1.5	5.2	16.4	16.1	15.8	15.6
FLUXNET-MTE SHF (W m^{-2})	−5.1	−5.5	−1.4	−4.4	18.2	18.2	16.3	16.2
GEWEX-SRB SW$_{net}$ (W m^{-2})	−1.6	−1.8	13	12.4	24.0	21.6	24.8	24.2
GEWEX-SRB LW$_{net}$ (W m^{-2})	1.1	0.8	5.6	3.8	13.4	12.3	14.1	13.1
CRU T_{2m} (K)	−0.41	−0.47	0.69	0.49	2.67	2.64	2.02	1.82
CRU Precipitation (mm yr^{-1})	102	101	94	92	50	50	54	54
GPCP Precipitation (mm yr^{-1})	38	37	18	16	47	40	51	50
GHCNDEX *TXx* (K)	0.80	0.60	2.25	1.67	6.00	6.00	/	/
HadEX2 *TXx* (K)	0.41	0.22	2.53	1.93	5.79	5.78	3.93	3.57
GHCNDEX *TNn* [K]	−4.70	−4.55	2.51	2.76	7.56	7.57	8.54	8.50
HadEX2 *TNn* [K]	−4.76	−4.60	1.37	1.58	6.92	6.92	5.42	5.35

[a]Regions with an observational coverage below 50% are excluded.
[b]Given the absence of monthly data for this product, the spatial RMSE is shown here.
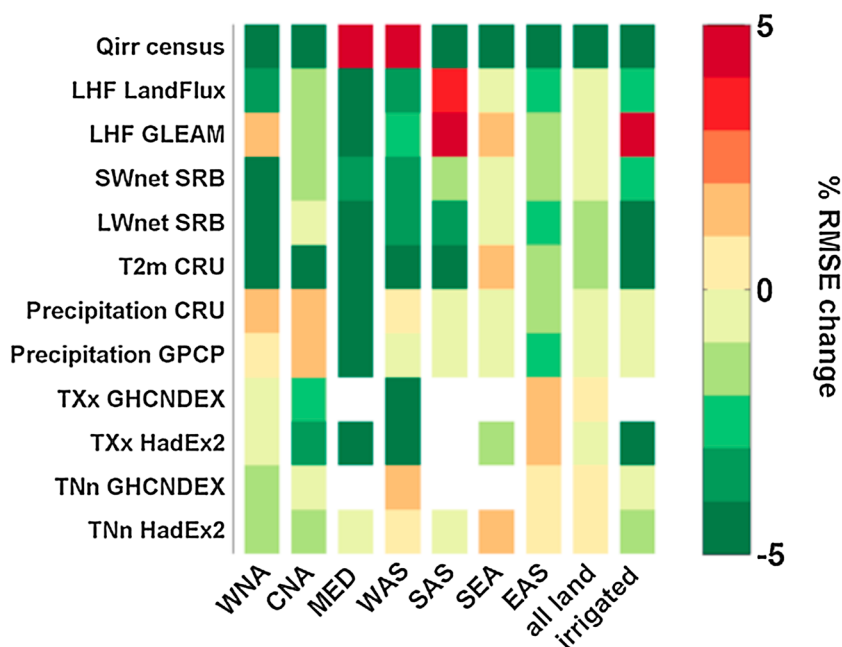
Figure 3. Added value of including irrigation. Percentage change in spatiotemporal root-mean-square error (RMSE) for the IRR ensemble relative to the CTL ensemble over different regions (x axis) and with respect to 12 observational products (y axis). Considered regions are the seven SREX regions defined in section 2.3 plus global land and global irrigated land. Observational products are for irrigation rates (census data), latent heat flux LHF (LandFlux-EVAL, GLEAM), surface net shortwave SW_{net} and longwave LW_{net} radiation (GEWEX-SRB), near-surface air temperature T_{mean} (CRU), precipitation (CRU and GPCP), monthly maximum daytime temperature TXx (GHCNDEX and HadEX2), and monthly minimum nighttime temperature TNn (GHCNDEX and HadEX2; see section 2.3 for a detailed description of these data sets). The RMSEs are computed for the ensemble mean, monthly climatology in every pixel, and subsequently averaged over the selected region (except for Q_{irr} for which we have only annual observations available). Regions with an observational coverage below 50% are marked in white. Note that we assumed $Q_{irr} = 0$ mm yr^{-1} in the CTL simulation.

over SAS in the IRR ensemble relative to the CTL ensemble. We note, however, that GLEAM and LandFlux-EVAL only indirectly account for irrigation influences on LHF, which adds to the uncertainty of assessments based on these products.

Overall, the results demonstrate that CESM is marked by substantial biases in terms of near-surface climate representation over land. The irrigation routine is, however, able to reproduce observed irrigation patterns, and including irrigation has a small yet robust beneficial effect on the representation of present-day near-surface climate in CESM. We therefore conclude that CESM is an appropriate tool to investigate the impact of irrigation on the climate.

3.2. Impact of Irrigation on the Mean Climate
3.2.1. Temperature and Turbulent Fluxes
Irrigation has a clear cooling effect on near-surface air temperature in irrigated regions (average impact of −0.20 K; see Table 3 and Figure 4a). The land cools especially over irrigated parts of WNA (−0.13 K), CNA (−0.08 K), MED (−0.24 K), WAS (−0.29 K), SAS (−0.28 K), SEA (−0.07 K), and EAS (−0.10 K). Locally, the annual mean cooling exceeds −0.18 K in each of these regions, and in SAS impacts exceeding −1.6 K are found. Moreover, the cooling mostly coincides with an increase in LHF and a decrease in SHF (Figures 4c and 4d). In section 3.4, we further investigate the processes underlying the obtained temperature impact.

Irrigation also induces remote temperature changes. Outside the irrigated areas, irrigation mostly leads to a cooling, except in the Sahara and Kazakhstan. The average irrigation impact on land is −0.05 K, consistent with estimates founds in other recent GCM studies (Table 3 and section 1).

According to our simulations, irrigation leads to an additional moisture input to the atmosphere of 418 km^3 yr^{-1}. 95% of this increase in evapotranspiration is realized over land and 81% over irrigated areas. Our evapotranspiration estimate is lower than that of previous modeling experiments (e.g., *Sacks et al.* [2009], 1233 km^3 yr^{-1}, and *Guimberteau et al.* [2012] 568 km^3 yr^{-1}]).

Table 3. Impact of the Irrigation on Various Climatological Values (IRR Minus CTL)[a]

| Physical Quantity (Units)	All Land		Irrigated Land	
	ABS	REL	ABS	REL
T_{2m} (K)	-0.05[b]	0.0	-0.20[b]	-0.1
Precipitation (mm yr^{-1})	-1.02	0.0	-2.02	0.5
ET (mm yr^{-1})	2.80[b]	2.5	47.10[b]	21.3
T_S (K)	-0.06[b]	0.0	-0.27[b]	-0.1
SW$_{net}$ (W m^{-2})	-0.20[b]	-0.3	-0.54[b]	-0.3
LW$_{net}$ (W m^{-2})	-0.27[b]	0.3	-1.74[b]	-1.9
LHF (W m^{-2})	0.22[b]	0.0	3.73[b]	21.2
SHF (W m^{-2})	-0.43[b]	-0.8	-3.01[b]	-6.3
Sea level pressure (hPa)	0.06[b]	0.0	0.09[b]	0.0
TXx (K)	-0.17[b]	0.1	-0.78[b]	-0.2
TNn (K)	0.11[b]	0.0	0.15[b]	0.1
CDD (d)	-0.12	0.0	-0.87[b]	-1.0
HWDI (—)	-0.35[b]	/	-1.53[b]	/

[a]ABS and REL denote the absolute and percentage change, respectively, of each given quantity.

[b]The changes significant at the 1% significance level (two-sided Wilcoxon signed rank test on ensemble mean, temporally averaged maps; see also *Lorenz et al.* [2016]).
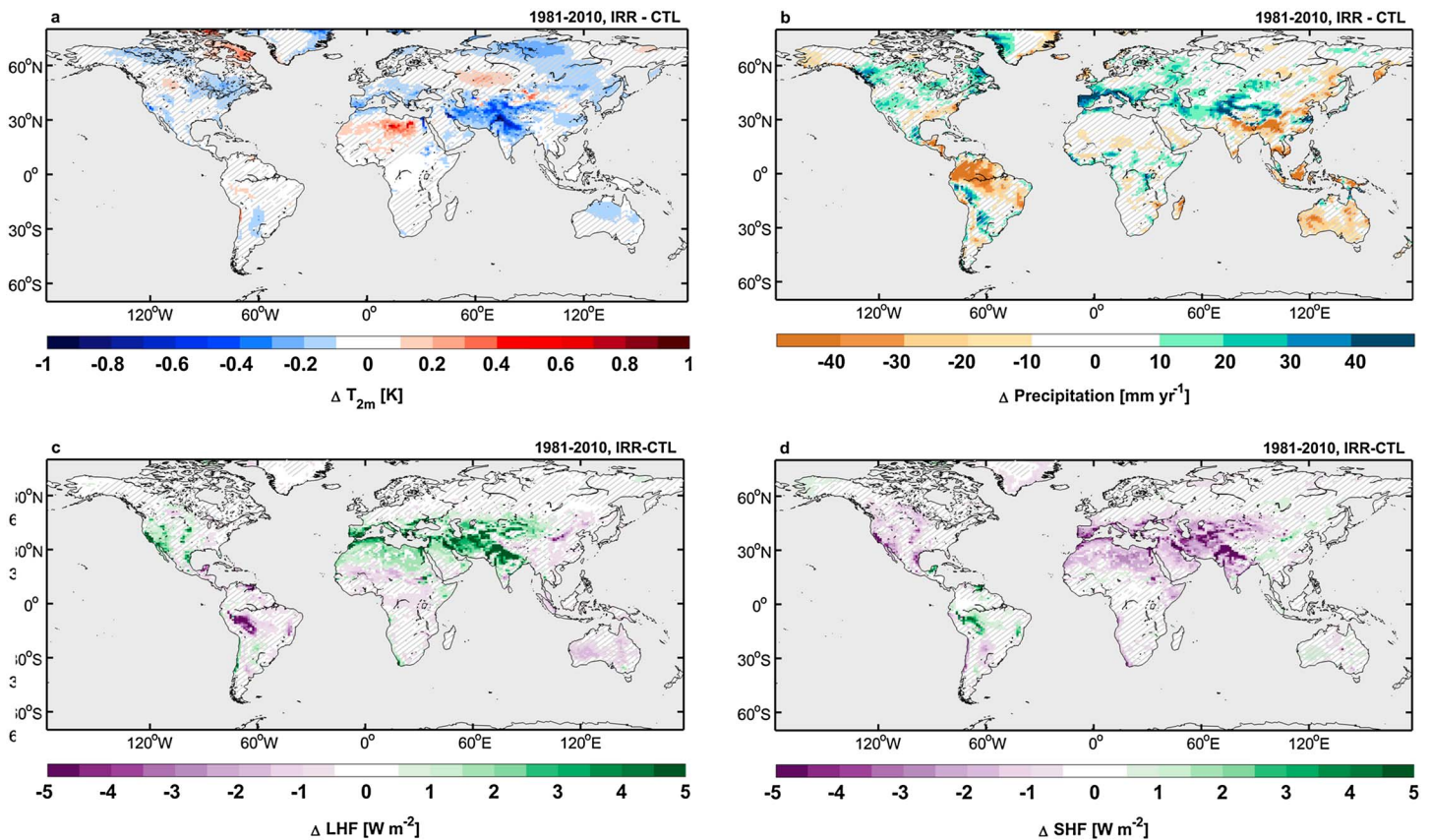
Figure 4. Impact of irrigation on (a) 2 m air temperature T_{2m}, (b) precipitation, (c) latent heat flux, LHF, and (d) sensible heat flux, SHF. Differences are based on the ensemble mean of each experiment for 1981–2010. Hatching denotes statistically insignificant changes at the 5% significance level (two-sided Wilcoxon signed rank test on annual mean of lumped ensemble members).
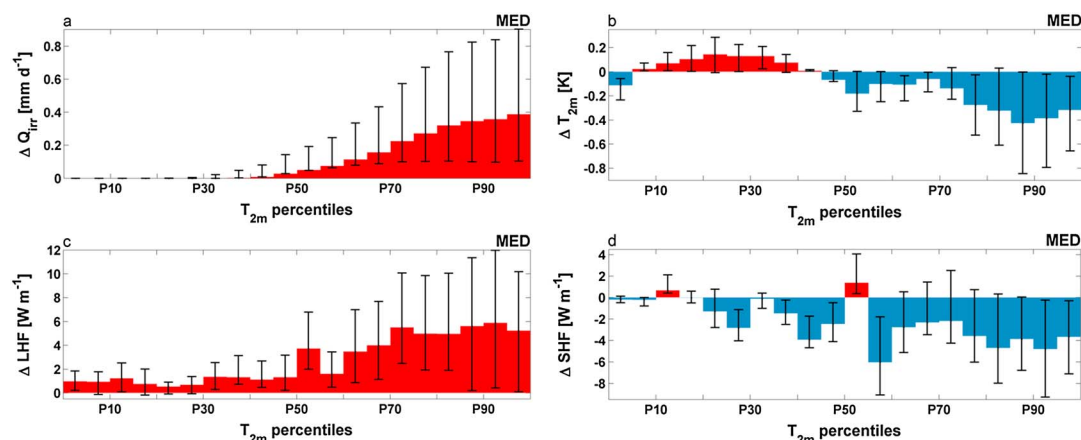
Figure 5. Impact of irrigation in southern Europe and the Mediterranean (MED) on binned (a) irrigation rates Q_{irr}, (b) 2 m air temperature T_{2m}, (c) latent heat flux, LHF, and (d) sensible heat flux, SHF. Each variable on the y axis was binned according to daily mean temperature using a bin width of 5%; bar heights indicate the change in bin median and whiskers the change in 25th and 75th percentile of spatially averaged, daily values. The binning was performed on the individual ensemble members and bin statistics were subsequently averaged over all ensemble members.
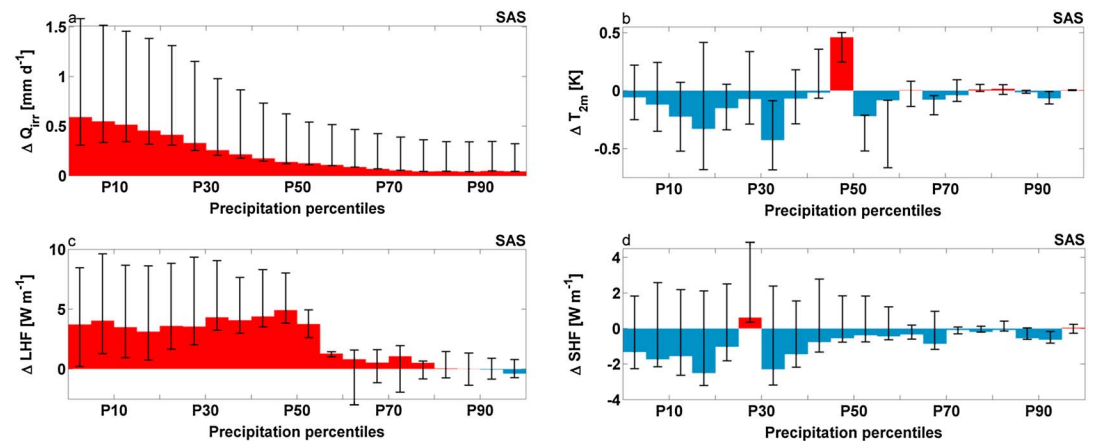
3.2.2. Precipitation

As a result of irrigation, modeled precipitation decreases by -1.02 mm yr^{-1} on average over land and by -2.02 mm yr^{-1} over all irrigated pixels (Table 3 and Figure 4b). Our perturbed initial condition ensemble suggests strong irrigation-induced precipitation increases over southern Europe and central Asia and to a lesser extend over North America. These changes may be ascribed to an intensification of the regional hydrological cycle. In contrast, a clear precipitation decrease is found in South and Southeast Asia due to a weakened monsoon circulation. Several irrigation modeling studies have indeed advanced that a reduced land sea contrast during spring delays the onset and/or decreases the intensity of the Indian summer monsoon [*Puma and Cook*, 2010; *Guimberteau et al.*, 2012; *de Vrese et al.*, 2016], thereby eliminating an initial positive contribution to precipitation from enhanced evapotranspiration [*Wei et al.*, 2013]. The substantial springtime cooling found over SAS in our simulations (section 3.4) corroborates this hypothesis.

By modifying large-scale circulation, irrigation may also lead to remote precipitation changes. For instance, as in *de Vrese et al.* [2016], our simulations indicate an irrigation-induced increase in precipitation over the Horn of Africa and the African Great Lakes region. However, this increase is much less pronounced in our simulations. Further, we find more pronounced remote changes in other regions, notably a strong drying over the Amazon basin and moderate precipitation reductions in Australia and along a substantial part of the Atlantic and East Pacific coastlines. Again, this is inconsistent with precipitation impacts reported in earlier studies [e.g., *Cook et al.*, 2011, 2015; *Krakauer et al.*, 2016; *de Vrese et al.*, 2016]. Likely, these differences can be attributed to differences in model setup, number of ensemble members, and the applied irrigation forcing [*Krakauer et al.*, 2016]. But also convective triggering remains a major source of uncertainty in current GCMs. This overall suggests that coordinated multimodel experiments are needed to identify robust impacts of irrigation on precipitation.

3.3. Asymmetric Response and Impact on Extremes

Our simulations show differential temperature changes during cold and warm days in response to irrigation. In the Mediterranean region, for instance, lower temperatures generally increase whereas high temperatures decrease (Figure 5b). Consequently, irrigation-induced cooling is 4.0 times stronger here during the 20% warmest days of the year compared to the average change. Similar effects are also found in South Asia, especially when binning ΔT_{2m} according to precipitation instead of temperature percentiles (Figure 6b). This indicates that the strongest climatic impacts occur during the dry periods of the monsoon cycle.

The primary reason for this behavior is rather straightforward: by design, irrigation will apply more water during periods with a substantial soil moisture deficit, i.e., during the hottest and/or driest period of the year (Figures 5a and 6a). During such periods climatic responses are thus expected to be strongest. In contrast, the temperature rise found for the lower MED percentiles cannot be caused by a change in evaporative fraction, as LHF values increase across all temperature percentiles whereas the SHF nearly always decreases

Figure 6. Same as Figure 5 but for South Asia (SAS) and with each variable on the *y* axis binned according to daily accumulated precipitation instead of daily mean temperature.

(Figures 5c and 5d). Other effects leading to enhanced net radiation available at the surface are therefore responsible for the higher temperatures in the IRR ensemble (see sections 2.5 and 3.5).

In addition to climatological extremes, irrigation may also induce hydrological extremes. In our simulations, where irrigation water is entirely removed from runoff, irrigation translates into substantial reductions in runoff under warm and/or dry conditions. In the Mediterranean region, low flows are the most affected, as irrigation is a summer phenomenon there. During the 20% warmest days of the year, irrigation in the Mediterranean requires 4.8 times more water than available through runoff, suggesting that in reality
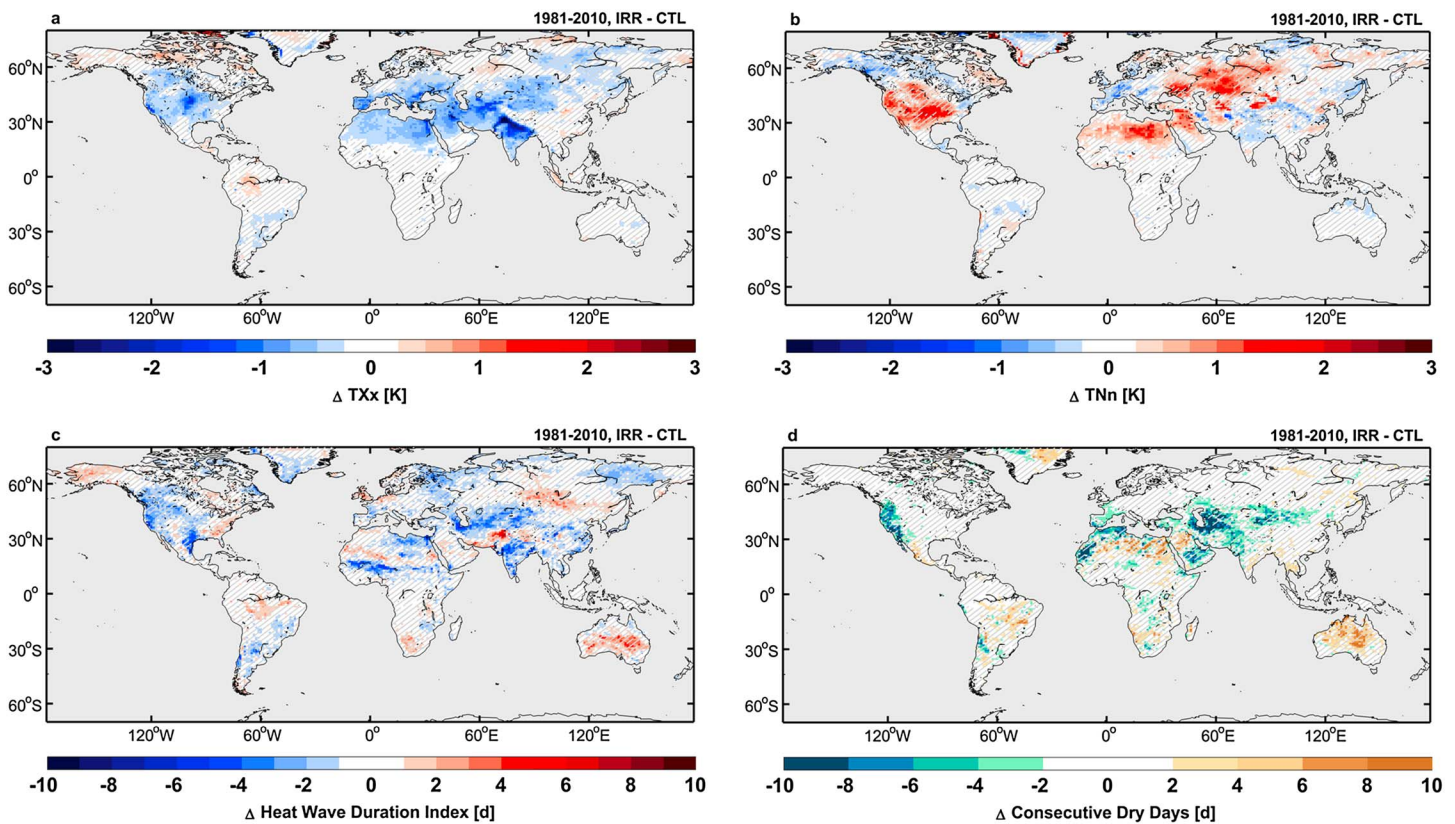
Figure 7. Impact of irrigation on (a) annual maximum daytime temperature, TXx, (b) annual minimum nighttime temperature, TNn, (c) heat wave duration index, HWDI, and (d) consecutive dry days, CDD. Differences are based on the ensemble mean of each experiment for 1981–2010. Hatching denotes statistically insignificant changes at the 5% significance level (two-sided Wilcoxon signed rank test on annual mean of lumped ensemble members).
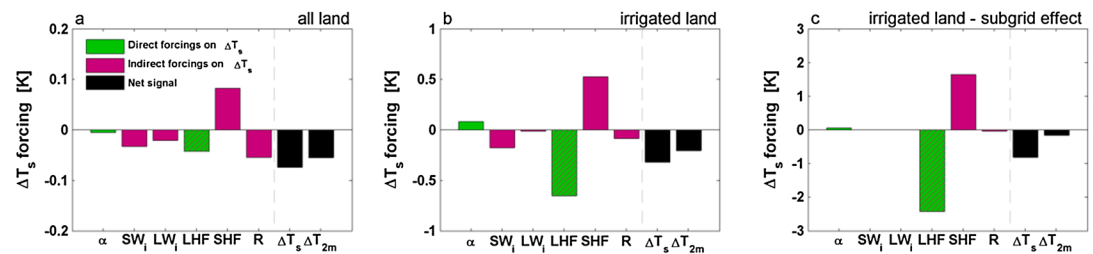
Figure 8. Irrigation-induced changes in surface temperatures. Individual direct (green), indirect (purple), and mixed (hatched) contributions to ΔT_s as described in equation (3) over (a) all land, (b) irrigated land, and (c) irrigated land - subgrid effect (all units K). Each contributing factor is indicated by its corresponding responsible parameter or flux component, with α denoting the change in T_s caused by a modified albedo, SW_i by changing incoming shortwave radiation, LW_i by changing incoming longwave radiation, LHF by changing evapotranspiration, SHF by changing sensible heat flux and R by changes in other components (subsurface heat flux and anthropogenic heat fluxes). The irrigation impact on T_{2m} is also shown for reference. Note the different y axis scales.

irrigation water is extracted from unsustainable sources during this period. This highlights the vulnerability of this region in terms of water resources, especially in the context of increased observed drought risk [*Gudmundsson and Seneviratne*, 2016] and projected reductions in water availability [*Orlowsky et al.*, 2014]. In contrast, South Asia experiences the driest conditions in spring when rivers are fed by meltwater from the Himalayas. Although much more intense than MED, irrigation therefore consumes only the equivalent of 68% of the total runoff during the 20% driest days of the year. Note, however, that our simulations do not differentiate between surface and groundwater sources for irrigation [*Leng et al.*, 2015]; therefore, a detailed analysis of irrigation impacts on water resources is not possible with the present model configuration.

The asymmetric response to irrigation translates into strong changes in temperature extremes: TXx consistently decreases over almost all land pixels, and locally by more than 3 K, whereas TNn generally increases, locally by more than 2 K (Figure 7). Averaged over irrigated land, the decrease in TXx (-0.78 K) is 3.8 times stronger than the cooling of the annual mean temperature (3.2 times over all land; Table 3). Our simulations furthermore demonstrate a considerable decrease in heat wave duration, as illustrated here by the change in the Heat Wave Duration Index (HWDI; Figure 7c). The irrigation-induced reduction in heat wave duration is consistent with the conclusions of previous studies [e.g., *Seneviratne et al.*, 2006; *Fischer et al.*, 2007; *Hirschi et al.*, 2010; *Miralles et al.*, 2014] that soil dessication is a key contributor to the development of extreme heat waves. Besides directly adding water to the irrigated soil column, changing precipitation patterns also modify soil moisture for the entire vegetated fractions. More specifically, by reducing the number of consecutive dry days (CDD) in irrigated regions (Figure 7d). Irrigation may thus shift an entire region from a soil moisture-limited toward an energy-limited evaporation regime and thereby render it less prone to extreme temperature variability [*Seneviratne et al.*, 2006, 2010; *Hirsch et al.*, 2014a].

3.4. Decomposing the Irrigation-Induced Surface Temperature Change

The six factors contributing to the net change in surface temperature ΔT_s (equation (3)) are shown in Figure 8 and are expressed in kelvin. Over irrigated land, the net temperature signal is dominated by the change in turbulent flux partitioning of the net surface radiation (Figure 8b; see also Figures 4c and 4d). A strong increase in LHF contributes to a lower ΔT_s by -0.65 K in these pixels and thereby forms the largest individual contribution to ΔT_s. This cooling effect is then partly offset by the warming influence of Δ SHF amounting up to 0.53 K (a reduced upward SHF leaves more energy available at the surface). Overall, the irrigation-induced cooling due to the increased evaporative fraction is consistent with *Cook et al.* [2015] but contrasts with *Sacks et al.* [2009] who attribute the irrigation effects mostly to changes in cloud cover and associated surface net radiation. *Sacks et al.* [2009] performed their experiments with an earlier version of the atmospheric model (CAM3), wherein convection is very sensitive to surface LHF changes. This may explain why cloud cover and radiative fluxes are much more affected in their simulations.

Other effects have only a minor influence on ΔT_s. Wet soils are darker and therefore reflect less incoming radiation, resulting in a direct positive contribution to ΔT_s from changing albedo of $+0.08$ K over irrigated regions. Note that since we prescribe vegetation phenology in our simulations, potential irrigation-induced changes in crop albedo (e.g., a decrease due to greening) are not captured. The remaining contributions to ΔT_s are all negative and originate from decreasing incoming shortwave (-0.18 K) and longwave (-0.01 K)
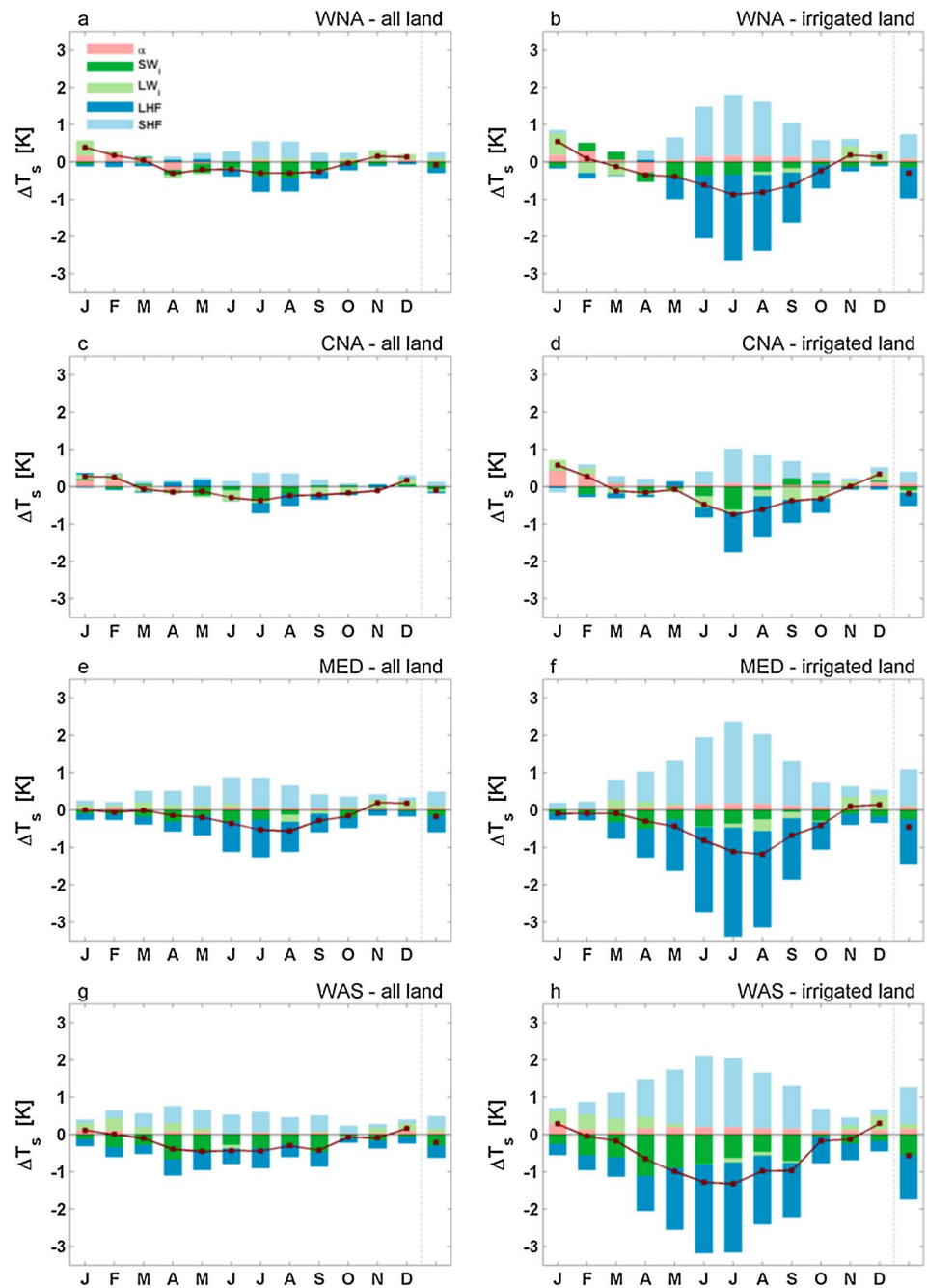
Figure 9. Seasonal cycle of irrigation-induced changes in surface temperatures. Monthly mean contributions to ΔT_s as described in equation (3) over (a, c, e, and g) all pixels and (b, d, f, and h) irrigated pixels of Western North America (WNA; Figures 9a and 9b), Central North America (CNA; Figures 9c and 9d), south Europe and Mediterranean (MED; Figures 9e and 9f), and West Asia (WAS; Figures 9g and 9h). The individual contributions are visualized as stacked bars, whereas the brown line shows the net T_s change. The impact on annual mean T_s is shown right of the grey line.

radiation caused by changing cloud cover and atmospheric temperature, and finally from a reduction in the residual heat flux (−0.08 K; Figure 8b).

As expected, irrigation impacts on T_s critically depend on irrigation extent. This is illustrated by comparing the impacts over irrigated land to those over all land (Figure 8a) and to the difference between the irrigated and rainfed crop tiles within grid cells of the IRR ensemble (Figure 8c). The temperature impact of irrigation is much larger over irrigated pixels compared to the rest of the total land area (Table 3), but the strongest impact on T_s is recorded on the subgrid scale; that is, irrigated crop tiles are on average −0.81 K colder compared to
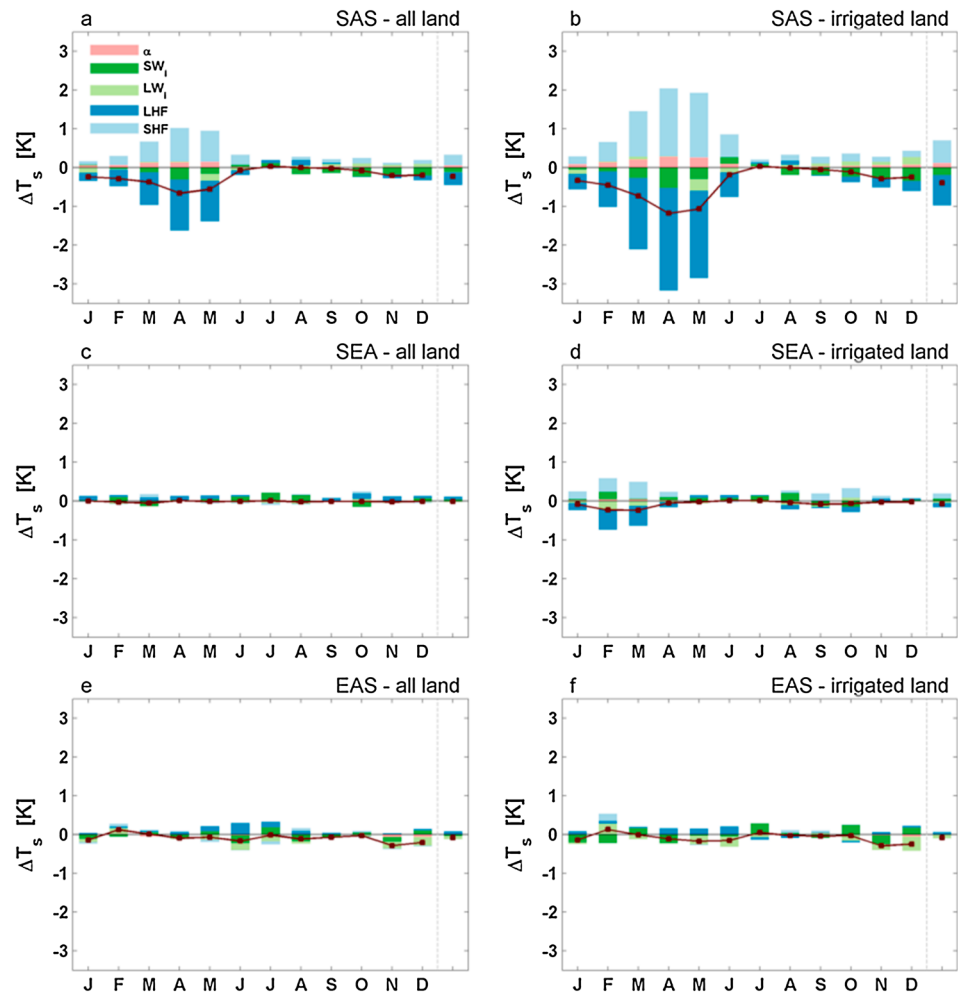
Figure 10. Same as Figure 9, but for (a, b) South Asia (SAS), (c, d) Southeast Asia (SEA), and (e, f) East Asia (EAS).

their rainfed counterpart within the same pixel (Figure 8c). Furthermore, due to the remote effects of irrigation (e.g., changes in the hydrological cycle, atmospheric circulation, and cloud cover) and the larger contribution of natural variability, the relative contribution of the other components also grows larger when considering all land pixels (Figure 8a). And again we find the largest individual contributions when comparing surface energy balance contributions at the subgrid scale. Note that in the latter case, contributions from changing incoming shortwave and longwave radiation are absent per definition, since both crop tiles receive the same atmospheric forcing. A more detailed description of grid-scale versus subgrid-scale effects is provided in section 3.5.

The irrigation influence on T_s is generally characterized by a clear seasonal pattern, with stronger cooling during the hottest and/or driest months. In particular, the strongest cooling effects occur during the boreal summer months over Northern Hemisphere midlatitude regions WNA, CNA, MED, and WAS (Figure 9). In South Asia, we find the strongest cooling during the dry springtime months, followed by a sharp decline at the time of the onset of the summer monsoon (Figures 10a and 10b). Interestingly, our results show a warming during boreal winter in WNA and CNA, consistent with the rise in TNn (Figures 9a–9d and 7b). This warming is predominantly caused by enhanced incoming longwave radiation and the wet soil albedo effect in January and February.

In contrast, no substantial influence is found over SEA and EAS, despite modeled irrigation amounts being roughly equal to WNA and CNA (Figures 2 and 10c–10f). This suggests that irrigation impacts critically depend on the background climate. When analyzing land climate interactions, typically three soil moisture regimes are considered: a wet and a dry regime, where soil moisture does not impact evapotranspiration variability,
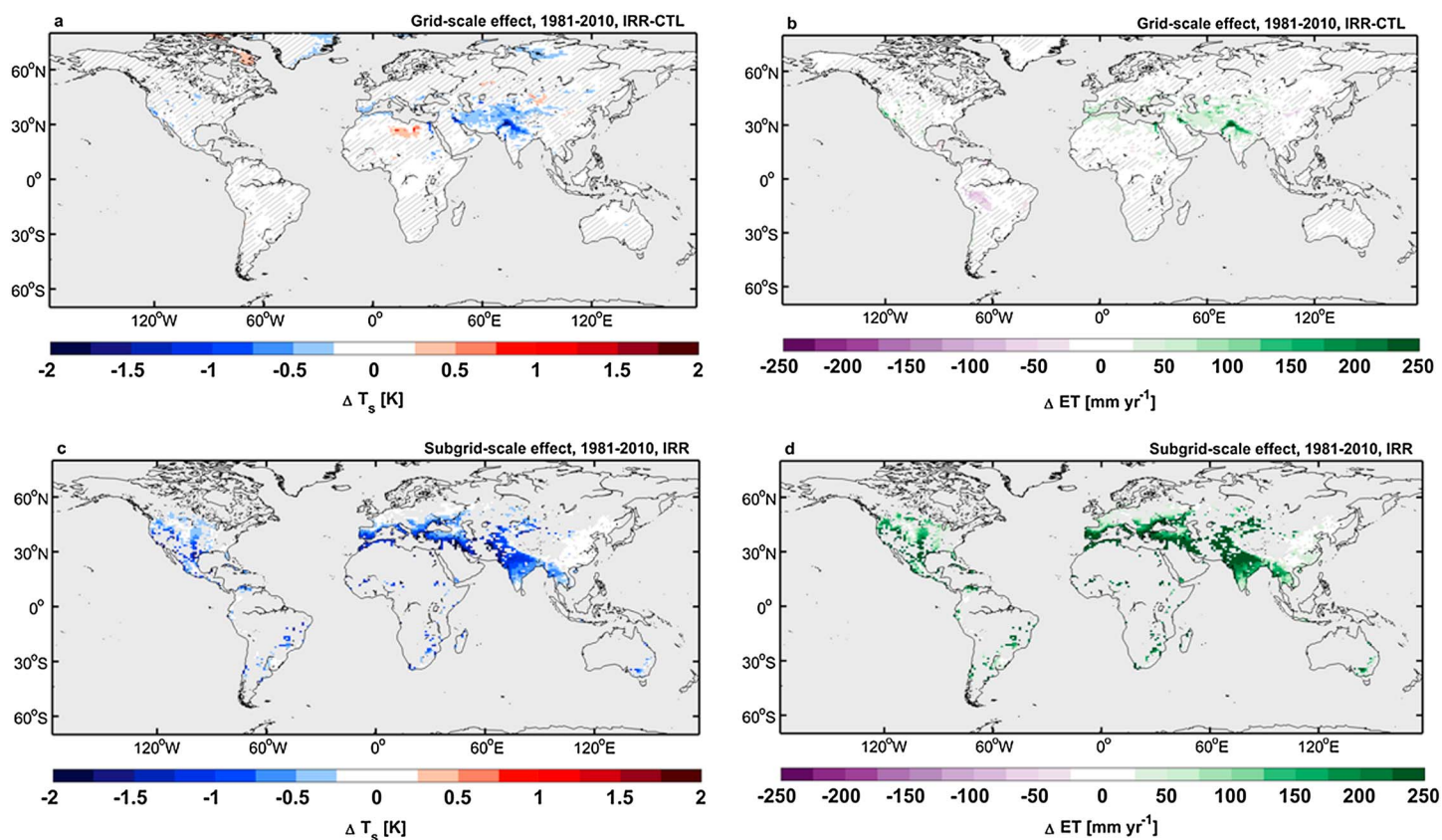
Figure 11. Impact of irrigation on grid-scale (a) surface temperature T_s and (b) evapotranspiration ET. Subgrid-scale differences in (c) T_s and (d) ET between the rainfed and irrigated crop tile in the IRR ensemble. Differences are based on the ensemble mean of each experiment for 1981–2010. Hatching denotes statistically insignificant changes at the 5% significance level (two-sided Wilcoxon signed rank test on annual mean of lumped ensemble members).

and a transitional regime where soil moisture strongly constrains evapotranspiration variability and thereby atmospheric responses [*Seneviratne et al.*, 2010]. In modeling studies this relationship is often evaluated by the covariance of soil moisture and temperature and termed land-atmosphere coupling strength [*Koster et al.*, 2006; *Hirsch et al.*, 2014a, 2014b]. Several modeling studies have indeed shown that WNA and CNA are characterized by strong land-atmosphere coupling (with evapotranspiration thus strongly depending on soil moisture content), whereas SEA and EAS generally display weaker coupling [e.g., *Koster et al.*, 2006; *Seneviratne et al.*, 2006]. This is confirmed by our simulations, which indicate that evapotranspiration increases with irrigation over WNA ($+8.86$ mm yr^{-1}) and CNA ($+3.24$ mm yr^{-1}), while it decreases over SEA ($+5.52$ mm yr^{-1}) and EAS ($+5.26$ mm yr^{-1}; Figure 4c). Injecting soil moisture via irrigation will thus lead to stronger climatic responses in WNA and CNA than in SEA and EAS.

3.5. Subgrid-Scale Impacts

Many land surface models nowadays represent land cover heterogeneity within grid cells through a mosaic of subgrid tiles with distinct physical, biogeochemical, and ecological characteristics [e.g., *Cook et al.*, 2011; *Guimberteau et al.*, 2012; *Oleson et al.*, 2013; *de Vrese et al.*, 2016]. Yet few studies have exploited the wealth of information available at the subgrid scale. Two noteworthy exceptions are the studies by *Malyshev et al.* [2015] and *Schultz et al.* [2016], who analyzed subgrid-scale output to assess local impacts of transient land cover changes and different land model configurations.

Here we use tiled model output to evaluate regional (grid-scale) versus local (subgrid-scale) influences of irrigation. In CLM4, up to 21 different surface tiles may occur within a single grid cell, including glacier, wetland, lake, urban, bare soil, and 16 PFTs. All tiles are placed on one single soil column, except for the irrigated crop tile which has a separate soil column. This enables the soils underneath rainfed and irrigated crop tiles to respond differently to an identical atmospheric forcing, a feature which is key for distinguishing subgrid-scale effects [*Schultz et al.*, 2016]. We consider surface radiative temperature T_s, which we compute from the longwave

radiation LW_{out} emitted by the surface using the Stefan-Boltzmann law (assuming constant $\epsilon = 1$). Since T_s is closer tied to the state of the land than to the state of the atmosphere, it is a more suitable measure than 2 m temperature for this type of analysis [*Malyshev et al.*, 2015]. In addition, we analyze the effects on evapotranspiration (ET), taken here as the sum of canopy evaporation, canopy transpiration, and ground evaporation.

Our results indicate that subgrid-scale influences of irrigation are much more pronounced than grid-scale effects (Figures 11a and 11c). Irrigated tiles are on average -0.50 K colder than their rainfed counterparts, whereas the average difference is only -0.12 K on the grid cell level. The subgrid cooling effect is particularly strong in MED and SAS, with T_s decreasing by -0.88 K and -0.68 K, respectively (relative to -0.17 K and -0.23 K at the grid scale). Furthermore, we again find that the effect is much smaller over SEA and EAS compared to WNA and CNA, confirming the importance of the background soil moisture regime when considering the climatic effects of irrigation. Differences are even more pronounced when comparing grid- and subgrid-scale ET values (Figures 11b and 11d). ET over irrigated tiles is 172 mm yr^{-1} higher compared to rainfed tiles, while it is only 16 mm yr^{-1} higher at the grid cell level. Even when scaling the subgrid irrigation effect on ET by the irrigated fraction within each grid cell, ET values are still higher than the total effect in SAS, suggesting that region-scale feedbacks caused by irrigation act to reduce ET from other land surface tiles.

This analysis overall suggests that climatic influences land of land use and land management changes may be much larger at the local scale then previously considered by grid-scale approaches. In fact, our current estimate of the subgrid-scale cooling effect can even be considered conservative. For T_s over the rainfed crop tile will generally be lower then if there would be no irrigation, since the tile undergoes an atmospheric forcing which already incorporates the prior effects of irrigation. However, care must be taken when assessing local irrigation impacts using subgrid-scale information, since the rainfed crop tile currently still shares a soil column with other PFTs. Unlike irrigated crops, rainfed crops thus compete for water with other vegetation types, which may influence the subgrid-scale SEB response to irrigation [*Schultz et al.*, 2016].

4. Discussion

Asymmetric temperature responses were already described for other land surface perturbations, for instance, regarding soil moisture deficits [*Jaeger and Seneviratne*, 2011; *Seneviratne et al.*, 2013] or surface albedo management [*Davin et al.*, 2014; *Wilhelm et al.*, 2015]. Also, the asymmetric temperature response to anthropogenic greenhouse gas emissions is well known [e.g., *Orlowsky and Seneviratne*, 2012; *Seneviratne et al.*, 2016]. Here we show that irrigation effects are highly dependent on the time of the year and that impacts on climate extremes are much more pronounced than influences on climatic averages. This is highly relevant for understanding the past and possible future climatic effects of irrigation, particularly since most research to date has focused only on the effects on the mean climate. The strong response also suggests that irrigation may have masked warming trends for temperature extremes in several regions of the world.

Our results also indicate that accounting for natural variability is of key importance to properly assess climatic impacts of land surface changes. In particular, it is clear that running ensemble GCM simulations is required to minimize spurious effects due to internal variability [*Lorenz et al.*, 2016]. For instance, when selecting random pairs of IRR and CTL simulations, the influence of irrigation on global land temperatures varies between -0.12 K and 0.01 K. The need to run ensemble simulations is even more pressing when assessing impacts on variables characterized by lower signal-to-noise ratios, such as precipitation. Natural variability has therefore likely influenced previous estimates of irrigation effects that were based on single-member simulations. Note that while we have tried to limit the influence of natural variability by conducting five-member ensembles with perturbed initial conditions, quantifying the remaining uncertainty related to natural variability lies beyond the scope of this study.

Although the present study was conducted with a state-of-the-art modeling system, and with greatest care for achieving realism, several future developments could potentially improve the understanding of the climatic influences of irrigation. First, we assumed year 2000 irrigation extent as input to the irrigation module in our otherwise transient simulations. Irrigation quantities applied during all years are thus representative for the year 2000, while in reality quantities increased during the simulation period (1981–2010). Currently supported versions of CLM cannot handle transient irrigation extent as irrigated crops are placed on a separate soil column with a fixed grid cell fraction. From version 5 onward, CLM will account for transient irrigation areas and volumes. Second, in this study we considered only one generic type of managed crop. From CLM4.5

onward, four types of irrigated crops are distinguished (corn, spring temperate cereal, winter temperate cereal, and soybean), but at the same time irrigation is only enabled in case of interactive carbon cycle modeling. This greatly increases the number of required spin-up years (on the order of thousands of years) and was therefore not considered in this study. Likewise, we do not account for water storage (e.g., rainwater tanks [*Demuzere et al.*, 2014]) nor for differences in irrigation techniques (e.g., flood, drip, or spray irrigation [*Lawston et al.*, 2015]) but rather extract the required irrigation amounts from runoff and apply it directly to the soil surface. As such we do not account for water supply limitations nor do we represent the various sources of irrigation water (e.g., runoff, reservoirs, or aquifers) and associated differences in soil water dynamics [e.g., *Tsakiris et al.*, 2013]. The poor representation of irrigation infrastructure, water availability, and of different crop types with their own growth cycle may lead to errors in the quantities and timing of irrigation. Other structural model deficiencies may add to uncertainties in the climatic response to irrigation. For instance, the empirically derived soil moisture stress functions utilized in most land surface models of this class represent a major source of uncertainty, and the same can be said of the parameterizations of convective triggering. Finally, we do not consider the role of ocean-atmosphere interactions in modulating the climatic impacts of irrigation, while these effects may be considerable [*Krakauer et al.*, 2016].

5. Conclusions

In this study we assessed the influence of irrigation on global climate and climate extremes for the period of 1981–2010 using the Community Earth System Model. Efforts were made to enhance the realism of the model experiments by (i) employing an irrigation parameterization which is able to compute realistic irrigation amounts based on local crop water demand and a global constraint, (ii) applying this water to a separate, irrigated crop tile while closing the hydrological balance, and (iii) reducing the effect of natural variability through ensemble simulations.

A comprehensive model evaluation demonstrates that the model reproduces observed irrigation rates, except over East and Southeast Asia. While the control ensemble is characterized by substantial biases in terms of near-surface climate representation, switching on the irrigation routine yields a small but robust improvement across a wide range of climatic variables and spatial domains. Averaged over irrigated land, we even note an improvement for all 13 considered observational products.

Irrigation reduces near-surface air temperatures in irrigated areas, but the overall cooling is relatively small (−0.20 K). Decomposing the temperature impact shows that the cooling is predominantly caused by an increase in evaporative fraction, with only a minor influence of reduced net radiation to the surface. Irrigation also typically generates an intensification of the hydrological cycle, except over South and Southeast Asia where a weakening of the monsoon circulation leads to substantial decreases in precipitation. While we also found remote precipitation changes, these effects may still be partly due to effects of natural variability. Furthermore, irrigation impacts critically depend on the background climate, as exemplified by the varying seasonal cycle of surface temperature responses and the role of the soil moisture regime in modulating temperature responses. Finally, we found that subgrid-scale influences of irrigation on surface temperatures and evapotranspiration are much stronger than grid-scale effects. This suggests that local effects of land management practices are far more important then previously thought.

Irrigation has a strong and spatially consistent impact on temperature extremes. Annual maximum daytime temperatures, for instance, decrease by −0.78 K on average over irrigated areas, while cold extremes are dampened as well due to atmospheric feedbacks. Besides applying most water when it is hot and dry, irrigation will also reduce the overall susceptibility of a region to land-atmosphere coupling and thereby its sensitivity to temperature variability.

Our findings overall underline that irrigation has substantially reduced human exposure to climate extremes so far and that future climate projections therefore need to account for irrigation effects.

References

Akkermans, T., W. Thiery, and N. P. M. Van Lipzig (2014), The regional climate impact of a realistic future deforestation scenario in the Congo Basin, *J. Clim.*, *27*(7), 2714–2734, doi:10.1175/JCLI-D-13-00361.1.

Biemans, H., C. Siderius, A. Mishra, and B. Ahmad (2016), Crop-specific seasonal estimates of irrigation-water demand in South Asia, *Hydrol. Earth Syst. Sci.*, *20*(5), 1971–1982, doi:10.5194/hess-20-1971-2016.

Bonfils, C., and D. Lobell (2007), Empirical evidence for a recent slowdown in irrigation-induced cooling, *Proc. Natl. Acad. Sci. U.S.A.*, *104*(34), 13,582–13,587, doi:10.1073/pnas.0700144104.

Boucher, O., G. Myhre, and A. Myhre (2004), Direct human influence of irrigation on atmospheric water vapour and climate, *Clim. Dyn.*, *22*, 597–603, doi:10.1007/s00382-004-0402-4.

Cook, B. I., M. J. Puma, and N. Y. Krakauer (2011), Irrigation induced surface cooling in the context of modern and increased greenhouse gas forcing, *Clim. Dyn.*, *37*(7-8), 1587–1600, doi:10.1007/s00382-010-0932-x.

Cook, B. I., S. P. Shukla, M. J. Puma, and L. S. Nazarenko (2015), Irrigation as an historical climate forcing, *Clim. Dyn.*, *44*, 1715–1730, doi:10.1007/s00382-014-2204-7.

Davin, E. L., S. I. Seneviratne, P. Ciais, A. Olioso, and T. Wang (2014), Preferential cooling of hot extremes from cropland albedo management, *Proc. Natl. Acad. Sci. U.S.A.*, *111*(27), 9757–9761, doi:10.1073/pnas.1317323111.

de Vrese, P., S. Hagemann, and M. Claussen (2016), Asian irrigation, African rain: Remote impacts of irrigation, *Geophys. Res. Lett.*, *43*, 3737–3745, doi:10.1002/2016GL068146.

Demuzere, M., A. Coutts, M. Göhler, A. Broadbent, H. Wouters, N. van Lipzig, and L. Gebert (2014), The implementation of biofiltration systems, rainwater tanks and urban irrigation in a single-layer urban canopy model, *Urban Clim.*, *10*, 148–170, doi:10.1016/j.uclim.2014.10.012.

Döll, P., and S. Siebert (2002), Global modeling of irrigation water requirements, *Water Resour. Res.*, *38*(4), 1037, doi:10.1029/2001WR000355.

Donat, M. G., L. V. Alexander, H. Yang, I. Durre, R. Vose, and J. Caesar (2013a), Global land-based datasets for monitoring climatic extremes, *Bull. Am. Meteorol. Soc.*, *94*(7), 997–1006, doi:10.1175/BAMS-D-12-00109.1.

Donat, M. G., et al. (2013b), Updated analyses of temperature and precipitation extreme indices since the beginning of the twentieth century: The HadEX2 dataset, *J. Geophys. Res. Atmos.*, *118*, 2098–2118, doi:10.1002/jgrd.50150.

Doughty, C. E., C. B. Field, and A. M. S. McMillan (2011), Can crop albedo be increased through the modification of leaf trichomes, and could this cool regional climate?, *Clim. Change*, *104*, 379–387, doi:10.1007/s10584-010-9936-0.

Fischer, E. M., S. I. Seneviratne, D. Lüthi, and C. Schär (2007), Contribution of land-atmosphere coupling to recent European summer heat waves, *Geophys. Res. Lett.*, *34*(6), L06707, doi:10.1029/2006GL029068.

Foley, J. A., et al. (2011), Solutions for a cultivated planet, *Nature*, *478*(7369), 337–42, doi:10.1038/nature10452.

Gudmundsson, L., and S. I. Seneviratne (2016), Anthropogenic climate change affects meteorological drought risk in Europe, *Environ. Res. Lett.*, *11*(4), 44005, doi:10.1088/1748-9326/11/4/044005.

Guimberteau, M., K. Laval, A. Perrier, and J. Polcher (2012), Global effect of irrigation and its impact on the onset of the Indian summer monsoon, *Clim. Dyn.*, *39*, 1329–1348, doi:10.1007/s00382-011-1252-5.

Haddeland, I., D. P. Lettenmaier, and T. Skaugen (2006), Effects of irrigation on the water and energy balances of the Colorado and Mekong river basins, *J. Hydrol.*, *324*, 210–223, doi:10.1016/j.jhydrol.2005.09.028.

Hanasaki, N., S. Kanae, T. Oki, K. Masuda, K. Motoya, N. Shirakawa, Y. Shen, and K. Tanaka (2008), An integrated model for the assessment of global water resources—Part 2: Applications and assessments, *Hydrol. Earth Syst. Sci.*, *12*(4), 1027–1037, doi:10.5194/hess-12-1027-2008.

Harris, I., P. D. Jones, T. J. Osborn, and D. H. Lister (2014), Updated high-resolution grids of monthly climatic observations—The CRU TS3.10 Dataset, *Int. J. Climatol.*, *34*(3), 623–642, doi:10.1002/joc.3711.

Helkowski, J. H. (2004), Global patterns of soil moisture and runoff: An assessment of water availability, MSc. thesis, University of Wisconsin - Madison, Wis.

Hirsch, A. L., A. J. Pitman, S. I. Seneviratne, J. P. Evans, and V. Haverd (2014a), Summertime maximum and minimum temperature coupling asymmetry over Australia determined using WRF, *Geophys. Res. Lett.*, *41*, 1546–1552, doi:10.1002/2013GL059055.

Hirsch, A. L., A. J. Pitman, and J. Kala (2014b), The role of land cover change in modulating the soil coupling strength over Australia, *Geophys. Res. Lett.*, *41*, 5883–5890, doi:10.1002/2014GL061179.

Hirschi, M., S. I. Seneviratne, V. Alexandrov, F. Boberg, C. Boroneant, O. B. Christensen, H. Formayer, B. Orlowsky, and P. Stepanek (2010), Observational evidence for soil-moisture impact on hot extremes in southeastern Europe, *Nat. Geosci.*, *4*(1), 17–21, doi:10.1038/ngeo1032.

Huffman, G. J., R. F. Adler, M. M. Morrissey, D. T. Bolvin, S. Curtis, R. Joyce, B. McGavock, and J. Susskind (2001), Global precipitation at one-degree daily resolution from multisatellite observations, *J. Hydrometeorol.*, *2*, 36–50.

Hurrell, J. W., J. J. Hack, D. Shea, J. M. Caron, and J. Rosinski (2008), A new sea surface temperature and sea ice boundary dataset for the community atmosphere model, *J. Clim.*, *21*(19), 5145–5153, doi:10.1175/2008JCLI2292.1.

Hurrell, J. W., et al. (2013), The Community Earth System Model: A framework for collaborative research, *Bull. Am. Meteorol. Soc.*, *94*(November 2012), 1339–1360, doi:10.1175/BAMS-D-12-00121.1.

Jacobs, L., O. Dewitte, J. Poesen, D. Delvaux, W. Thiery, and M. Kervyn (2016a), The Rwenzori Mountains, a landslide-prone region?, *Landslides*, *13*, 519–536, doi:10.1007/s10346-015-0582-5.

Jacobs, L., J. Maes, K. Mertens, J. Sekajugo, W. Thiery, N. P. M. van Lipzig, J. Poesen, M. Kervyn, and O. Dewitte (2016b), Reconstruction of a flash flood event through a multi-hazard approach: Focus on the Rwenzori Mountains, Uganda, *Nat. Hazards*, *84*(2), 851–876, doi:10.1007/s11069-016-2458-y.

Jaeger, E. B., and S. I. Seneviratne (2011), Impact of soil moisture-atmosphere coupling on European climate extremes and trends in a regional climate model, *Clim. Dyn.*, *36*, 1919–1939, doi:10.1007/s00382-010-0780-8.

Jones, P. W. (1999), First- and second-order conservative remapping schemes for grids in spherical coordinates, *Mon. Weather Rev.*, *127*(9), 2204–2210.

Juang, J.-Y., G. Katul, M. Siqueira, P. Stoy, and K. Novick (2007), Separating the effects of albedo from eco-physiological changes on surface temperature along a successional chronosequence in the southeastern United States, *Geophys. Res. Lett.*, *34*(21), L21408, doi:10.1029/2007GL031296.

Jung, M., et al. (2010), Recent decline in the global land evapotranspiration trend due to limited moisture supply, *Nature*, *467*(7318), 951–954, doi:10.1038/nature09396.

Koster, R. D., et al. (2006), GLACE: The Global Land–Atmosphere Coupling Experiment. Part I: Overview, *J. Hydrometeorol.*, *7*, 611–625, doi:10.1175/JHM511.1.

Krakauer, N. Y., M. J. Puma, B. I. Cook, P. Gentine, and L. Nazarenko (2016), Ocean-atmosphere interactions modulate irrigation's climate impacts, *Earth Syst. Dyn.*, *7*, 863–876, doi:10.5194/esd-7-863-2016.

Kueppers, L. M., and M. A. Snyder (2012), Influence of irrigated agriculture on diurnal surface energy and water fluxes, surface climate, and atmospheric circulation in California, *Clim. Dyn.*, *38*(5–6), 1017–1029, doi:10.1007/s00382-011-1123-0.

Kueppers, L. M., M. A. Snyder, and L. C. Sloan (2007), Irrigation cooling effect: Regional climate forcing by land-use change, *Geophys. Res. Lett.*, *34*, L03703, doi:10.1029/2006GL028679.

Lawrence, D. M., et al. (2011), Parameterization improvements and functional and structural advances in version 4 of the Community Land Model, *J. Adv. Model. Earth Syst.*, *3*, M03001, doi:10.1029/2011MS000045.

Lawrence, D. M., et al. (2016), The Land Use Model Intercomparison Project (LUMIP) contribution to CMIP6: Rationale and experimental design, *Geosci. Model Dev.*, *9*, 2973–2998, doi:10.5194/gmd-2016-76.

Lawston, P. M., J. A. Santanello, B. F. Zaitchik, and M. Rodell (2015), Impact of irrigation methods on land surface model spinup and initialization of WRF forecasts, *J. Hydrometeorol.*, *16*, 1135–1154, doi:10.1175/JHM-D-14-0203.1.

Leng, G., M. Huang, Q. Tang, W. J. Sacks, H. Lei, and L. R. Leung (2013), Modeling the effects of irrigation on land surface fluxes and states over the conterminous United States: Sensitivity to input data and model parameters, *J. Geophys. Res. Atmospheres*, *118*, 9789–9803, doi:10.1002/jgrd.50792.

Leng, G., M. Huang, Q. Tang, and R. Lueng (2015), A modeling study of irrigation effects on global surface water and groundwater resources under a changing climate, *J. Adv. Model. Earth Syst.*, *7*, 1285–1304, doi:10.1002/2013MS000282.

Lobell, D., G. Bala, A. Mirin, T. Phillips, R. Maxwell, and D. Rotman (2009), Regional differences in the inuence of irrigation on climate, *J. Clim.*, *22*(8), 2248–2255, doi:10.1175/2008JCLI2703.1.

Lobell, D. B., G. Bala, and P. B. Duffy (2006a), Biogeophysical impacts of cropland management changes on climate, *Geophys. Res. Lett.*, *33*, L06708, doi:10.1029/2005GL025492.

Lobell, D. B., G. Bala, C. Bonfils, and P. B. Duffy (2006b), Potential bias of model projected greenhouse warming in irrigated regions, *Geophys. Res. Lett.*, *33*, L13709, doi:10.1029/2006GL026770.

Lorenz, R., A. J. Pitman, and S. A. Sisson (2016), Does Amazonian deforestation cause global effects: Can we be sure?, *J. Geophys. Res. Atmos.*, *121*, 5567–5584, doi:10.1002/2015JD024357.

Lu, Y., and L. Kueppers (2015a), Increased heat waves with loss of irrigation in the United States, *Environ. Res. Lett.*, *10*(6), 64010, doi:10.1088/17489326/10/6/064010.

Lu, Y., J. Jin, and L. M. Kueppers (2015b), Crop growth and irrigation interact to influence surface fluxes in a regional climate-cropland model (WRF3.3-CLM4crop), *Clim. Dyn.*, *45*(11-12), 3347–3363, doi:10.1007/s00382-015-2543-z.

Luyssaert, S., et al. (2014), Land management and land-cover change have impacts of similar magnitude on surface temperature, *Nat. Clim. Change*, *4*(5), 389–393, doi:10.1038/nclimate2196.

Malyshev, S., E. Shevliakova, R. J. Stouffer, and S. W. Pacala (2015), Contrasting local versus regional effects of land-use-change-induced heterogeneity on historical climate: Analysis with the GFDL Earth System Model, *J. Clim.*, *28*(13), 5448–5469, doi:10.1175/JCLI-D-14-00586.1.

Miralles, D. G., T. RH Holmes, R. AM De J., J. H. Gash, A. GCA Meesters, and A. J. Dolman (2011), Global land-surface evaporation estimated from satellite-based observations, *Hydrol. Earth Syst. Sci.*, *15*(2), 453–469, doi:10.5194/hess-15-453-2011.

Miralles, D. G., A. J. Teuling, C. C. V. Heerwaarden, and J. Vila-Guerau de Arellano (2014), Mega-heatwave temperatures due to combined soil desiccation and atmospheric heat accumulation, *Nat. Geosci.*, *7*(5), 345–349, doi:10.1038/ngeo2141.

Mueller, B., et al. (2013), Benchmark products for land evapotranspiration: LandFlux-EVAL multi-data set synthesis, *Hydrol. Earth Syst. Sci.*, *17*(10), 3707–3720, doi:10.5194/hess-17-3707-2013.

Oleson, K. W., D. M. Lawrence, B. Gordon, M. G. Flanner, E. Kluzek, L. J. Peter, S. Levis, S. C. Swenson, and P. E. Thornton (2010), Technical description of version 4.0 of the Community Land Model (CLM), *Tech. Rep. NCAR/TN-478+STR*, Natl. Center for Atmos. Res., doi:10.5065/D6FB50WZ. [Available at http://www.cesm.ucar.edu/models/ccsm4.0/clm/CLM4_Tech_Note.pdf.]

Oleson, K. W., et al. (2013), Technical description of version 4.5 of the Community Land Model (CLM), *Tech. Rep.*, Natl. Center for Atmos. Res. [Available at http://www.cesm.ucar.edu/models/cesm1.2/clm/CLM45_Tech_Note.pdf.]

Orlowsky, B., and S. I. Seneviratne (2012), Global changes in extreme events: Regional and seasonal dimension, *Clim. Change*, *110*, 669–696, doi:10.1007/s10584-011-0122-9.

Orlowsky, B., A. Y. Hoekstra, L. Gudmundsson, and S. I. Seneviratne (2014), Today's virtual water consumption and trade under future water scarcity, *Environ. Res. Lett.*, *9*(7), 74007, doi:10.1088/1748-9326/9/7/074007.

Perkins, S. E., and E. M. Fischer (2013), The usefulness of different realizations for the model evaluation of regional trends in heat waves, *Geophys. Res. Lett.*, *40*(21), 5793–5797, doi:10.1002/2013GL057833.

Pongratz, J., T. Raddatz, C. H. Reick, M. Esch, and M. Claussen (2009a), Radiative forcing from anthropogenic land cover change since A.D. 800, *Geophys. Res. Lett.*, *36*, L02709, doi:10.1029/2008GL036394.

Pongratz, J., C. H. Reick, T. Raddatz, and M. Claussen (2009b), Effects of anthropogenic land cover change on the carbon cycle of the last millennium, *Global Biogeochem. Cycles*, *23*, GB4001, doi:10.1029/2009GB003488.

Puma, M. J., and B. I. Cook (2010), Effects of irrigation on global climate during the 20th century, *J. Geophys. Res.*, *115*, D16120, doi:10.1029/2010JD014122.

Sacks, W. J., B. I. Cook, N. Buenning, S. Levis, and J. H. Helkowski (2009), Effects of global irrigation on the near-surface climate, *Clim. Dyn.*, *33*, 159–175, doi:10.1007/s00382-008-0445-z.

Saeed, F., S. Hagemann, and D. Jacob (2009), Impact of irrigation on the South Asian summer monsoon, *Geophys. Res. Lett.*, *36*(20), 1–7, doi:10.1029/2009GL040625.

Saeed, F., S. Hagemann, S. Saeed, and D. Jacob (2013), Influence of mid-latitude circulation on upper Indus basin precipitation: The explicit role of irrigation, *Clim. Dyn.*, *40*(1), 21–38, doi:10.1007/s00382-012-1480-3.

Schultz, N., X. Lee, P. J. Lawrence, D. M. Lawrence, and L. Zhao (2016), Assessing the use of subgrid land model output to study impacts of land cover change, *J. Geophys. Res. Atmos.*, *121*, 1–29, doi:10.1002/2014JE004627.

Seneviratne, S. I., D. Lüthi, M. Litschi, and C. Schär (2006), Land-atmosphere coupling and climate change in Europe, *443*(7108), 205–209, doi:10.1038/nature05095.

Seneviratne, S. I., T. Corti, E. L. Davin, M. Hirschi, E. B. Jaeger, I. Lehner, B. Orlowsky, and A. J. Teuling (2010), Investigating soil moisture-climate interactions in a changing climate: A review, *Earth Sci. Rev.*, *99*(3-4), 125–161, doi:10.1016/j.earscirev.2010.02.004.

Seneviratne, S. I., et al. (2012), Changes in climate extremes and their impacts on the natural physical environment, in *Managing the Risks of Extreme Events and Disasters to Advance Climate Change Adaptation*, edited by C. B. Field et al., pp. 109–230, Cambridge Univ. Press, Cambridge, U. K.

Seneviratne, S. I., et al. (2013), Impact of soil moisture-climate feedbacks on CMIP5 projections: First results from the GLACE-CMIP5 experiment, *Geophys. Res. Lett.*, *40*, 5212–5217, doi:10.1002/grl.50956.

Seneviratne, S. I., M. G. Donat, A. J. Pitman, R. Knutti, and R. L. Wilby (2016), Allowable CO_2 emissions based on regional and impact-related climate targets, *529*, 477–483, doi:10.1038/nature16542.

Shiklomanov, I. A. (2000), Appraisal and assessment of world water resources, *Water Int.*, *25*(1), 11–32, doi:10.1080/02508060008686794.

Siebert, S., and P. Döll (2007), Irrigation water use A global perspective, in *Global Change: Enough Water for all?*, edited by J. Lozán et al., pp. 104–107, Universität Hamburg, doi:10.1029/2001WR000355.D. [Available at https://www.uni-frankfurt.de/45217784/Siebert_Doell_2007_incl_cover.pdf.]

Siebert, S, P Döll, J Hoogeveen, J.-M. Faures, K Frenken, and S Feick (2005), Development and validation of the global map of irrigation areas, *Hydrol. Earth Syst. Sci.*, *9*, 535–547, doi:10.5194/hessd-2-1299-2005.

Stackhouse, P. W., S. K. Gupta, S. J. Cox, T. Zhang, J. C. Mikovitz, and L. M. Hinkelman (2011), 24.5-year SRB data set released, *GEWEX News*, *21*(1), 10–12.

Thiery, W., A. Martynov, F. Darchambeau, J.-P. Descy, P.-D. Plisnier, L. Sushama, and N. P. M. van Lipzig (2014a), Understanding the performance of the FLake model over two African Great Lakes, *Geosci. Model Dev.*, *7*(1), 317–337, doi:10.5194/gmd-7-317-2014.

Thiery, W., et al. (2014b), LakeMIP Kivu: Evaluating the representation of a large, deep tropical lake by a set of 1-dimensional lake models, *Tellus A*, *66*, 21,390, doi:10.3402/tellusa.v66.21390.

Thiery, W., E. L. Davin, H.-J. Panitz, M. Demuzere, S. Lhermitte, and N. P. M. van Lipzig (2015), The impact of the African Great Lakes on the regional climate, *J. Clim.*, *28*, 4061–4085, doi:10.1175/JCLI-D-14-00565.1.

Thiery, W., E. L. Davin, S. I. Seneviratne, K. Bedka, S. Lhermitte, and N. P. M. van Lipzig (2016), Hazardous thunderstorm intensification over Lake Victoria, *Nat. Commun.*, *7*, 12786, doi:10.1038/ncomms12786.

Tsakiris, G., et al. (2013), A system-based paradigm of drought analysis for operational management, *Water Resour. Manage.*, *27*(15), 5281–5297, doi:10.1007/s11269-013-0471-4.

Van Tricht, K., S. Lhermitte, J. T. M. Lenaerts, I. V. Gorodetskaya, T. S. L'Ecuyer, B. Noël, M. R. van den Broeke, D. D. Turner, and N. P. M. van Lipzig (2016), Clouds enhance Greenland ice sheet meltwater runoff, *Nat. Commun.*, *7*, 10266, doi:10.1038/ncomms10266.

Vanden Broucke, S., S. Luyssaert, E. Davin, I. Janssens, and N. Van Lipzig (2015), Temperature decomposition of paired site observations reveals new insights in climate models' capability to simulate the impact of LUC, *J. Geophys. Res. Atmos.*, *120*, 5417–5436, doi:10.1002/2015JD023095.

Wei, J., P. A. Dirmeyer, D. Wisser, M. G. Bosilovich, and D. M. Mocko (2013), Where does the irrigation water go? An estimate of the contribution of irrigation to precipitation using MERRA, *J. Hydrometeorol.*, *14*(1), 275–289, doi:10.1175/JHM-D-12-079.1.

Wilhelm, M., E. L. Davin, and S. I. Seneviratne (2015), Climate engineering of vegetated land for hot extremes mitigation: An Earth system model sensitivity study, *J. Geophys. Res. Atmos.*, *120*, 2612–2623, doi:10.1002/2014JD022293.

Wisser, D., B. M. Fekete, C. J. Vörösmarty, and A. H. Schumann (2010), Reconstructing 20th century global hydrography: A contribution to the Global Terrestrial Network- Hydrology (GTN-H), *Hydrol. Earth Syst. Sci.*, *14*, 1–24, doi:10.5194/hessd-6-2679-2009.